THE JOURNAL OF PHYSICAL CHEMISTRY A

Article

pubs.acs.org/JPCA

Two HCl-Elimination Channels and Two CO-Formation Channels Detected with Time-Resolved Infrared Emission upon Photolysis of Acryloyl Chloride [$CH_2CHC(O)Cl$] at 193 nm

Pei-Wen Lee,[†] Preston G. Scrape,[‡] Laurie J. Butler,*[,‡] and Yuan-Pern Lee*[,†,§]

[†]Department of Applied Chemistry and Institute of Molecular Science, National Chiao Tung University, Hsinchu 30010, Taiwan

[‡]Department of Chemistry, The University of Chicago, Chicago, Illinois 60637, United States

[§]Institute of Atomic and Molecular Sciences, Academia Sinica, Taipei 10617, Taiwan

Supporting Information

ABSTRACT: Following photodissociation of gaseous acryloyl chloride, $CH_2CHC(O)Cl$, at 193 nm, temporally resolved vibration−rotational emission spectra of HCl ($v \leq 7$, $J \leq 35$) in region 2350−3250 cm^{-1} and of CO ($v \leq 4$, $J \leq 67$) in region 1865−2300 cm^{-1} were recorded with a step-scan Fourier-transform spectrometer. The HCl emission shows a minor low-J component for $v \leq 4$ with average rotational energy E_{rot} = 9 ± 3 kJ mol^{-1} and vibrational energy E_{vib} = 28 ± 7 kJ mol^{-1} and a major high-J component for $v \leq 7$ with average rotational energy E_{rot} = 36 ± 6 kJ mol^{-1} and vibrational energy E_{vib} = 49 ± 9 kJ mol^{-1}; the branching ratio of these two channels is ∼0.2:0.8. Using electronic structure calculations to characterize the transition states and each intrinsic reaction coordinate, we find that the minor pathway corresponds to the four-center HCl-elimination of $CH_2ClCHCO$ following a 1,3-Cl-shift of $CH_2CHC(O)Cl$, whereas the major pathway corresponds to the direct four-center HCl-elimination of $CH_2CHC(O)Cl$. Although several channels are expected for CO produced from the secondary dissociation of C_2H_3CO and $H_2C{=}C{=}C{=}O$, each produced from two possible dissociation channels of $CH_2CHC(O)Cl$, the CO emission shows a near-Boltzmann rotational distribution with average rotational energy E_{rot} = 21 ± 4 kJ mol^{-1} and average vibrational energy E_{vib} = 10 ± 4 kJ mol^{-1}. Consideration of the branching fractions suggests that the CO observed with greater vibrational excitation might result from secondary decomposition of $H_2C{=}C{=}C{=}O$ that was produced via the minor low-J HCl-elimination channel, while the internal state distributions of CO produced from the other three channels are indistinguishable. We also introduce a method for choosing the correct point along the intrinsic reaction coordinate for a roaming HCl elimination channel to generate a Franck−Condon prediction for the HCl vibrational energy.

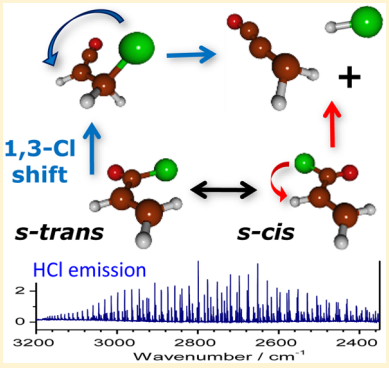

1. INTRODUCTION

Acryloyl chloride ($CH_2CHC(O)Cl$, also known as propenoyl chloride or acrylic acid chloride) is the simplest unsaturated chlorocarbonyl compound. It serves as an excellent substrate for cross-metathesis in various polymerization, biological, and medical applications.[1−4] Because of its enone ($C{=}C{-}C{=}O$) functional group, acryloyl chloride exhibits rich photochemistry. Extensive experimental investigations on the photolysis of $CH_2CHC(O)Cl$ have been reported.[5−10] The major photodissociation channel is the fission of its C−Cl bond to produce a C_2H_3CO radical, which is also a crucial intermediate in reactions between O atom and propargyl (C_3H_3) radical in combustion and atmospheric chemistry.[11]

Szpunar et al. investigated the dynamics of photodissociation of $CH_2CHC(O)Cl$ in a molecular beam with light at 193 nm using photofragment-translational spectroscopy.[7] They observed two C−Cl fission channels that produced Cl + C_2H_3CO with large and small kinetic energies and assigned them to dissociation on the excited and ground electronic surfaces, respectively. The C_2H_3CO radicals produced in both channels had sufficient internal energy to undergo secondary decomposition so that only products C_2H_3 + CO, not C_2H_3CO, were detected. A minor channel to form propadienone ($H_2C{=}C{=}C{=}O$) and HCl via four-center HCl-elimination was also observed; the branching ratio of this channel was estimated to be ∼25%. Lau et al. excited $CH_2CHC(O)Cl$ at 235 nm, at which most C_2H_3CO fragment is stable, and employed two-dimensional velocity-map imaging to determine the barrier height for the decomposition of C_2H_3CO to C_2H_3 + CO to be ∼96 kJ mol^{-1}.[8] Three conformers of C_2H_3CO were predicted to be stable: *s-cis*- and *s-trans*-3-propenalyl radicals (designated $CH_2C\dot{H}O$ in this

Special Issue: 100 Years of Combustion Kinetics at Argonne: A Festschrift for Lawrence B. Harding, Joe V. Michael, and Albert F. Wagner

Received: December 12, 2014
Revised: January 29, 2015

DOI: 10.1021/jp512376a
J. Phys. Chem. A XXXX, XXX, XXX−XXX

paper) with the carbonyl group *cis*- and *trans*- with respect to the CH_2 group, respectively, and 3-propenonyl (designated $\cdot CH_2CHCO$ in this paper) with a nearly linear CCO group.[12] Because of the similarity in energy, they employed light at 157 nm to photoionize all isomeric C_2H_3CO fragments formed on photodissociation of $CH_2CHC(O)Cl$ at 235 nm; no information about the conformation of the C_2H_3CO fragments was available. In this paper we indicate this radical as C_2H_3CO when the conformation is unspecified.

Yang et al. employed a step-scan Fourier-transform infrared (FTIR) spectrometer to detect emission of the photolysis products CO and HCl produced upon excitation of $CH_2CHC(O)Cl$ at 193 nm.[10] The vibrational and rotational temperatures and average energies of photofragments CO and HCl were determined on analyzing emission of vibrationally excited photofragments of CO ($v \leq 5$) and HCl ($v \leq 6$), but the distributions of internal states were not explicitly reported, and the observed spectra deviate significantly from their simulated spectra; only single Boltzmann distributions of internal states of HCl and of CO were reported.

Wu et al. employed a step-scan FTIR spectrometer to detect the absorption of photolysis products upon excitation of $CH_2CHC(O)Cl$ at 193 nm in a CH_3CN solution;[9] they observed an intense feature near 2128 cm^{-1} with lifetime ~280 μs and assigned it to 3-chloro-1-propen-1-one, $CH_2ClCHCO$, produced in a stepwise mechanism involving dissociation and recombination. A weak line near 1813 cm^{-1} that decayed within a few μs was also observed and assigned to $CH_2C\dot{H}CO$.

Pietri et al. used light of wavelength ≥310 nm to photolyze $CH_2CHC(O)Cl$ isolated in an Ar matrix at 10 K and observed IR absorption of only $CH_2ClCHCO$ with a characteristic broad feature near 2139 cm^{-1}; no absorption was ascribable to $CH_2C\dot{H}CO$.[6] Although they ascribed the mechanism of formation to involve a 1,3-Cl migration, 3-chloro-1-propen-1-one ($CH_2ClCHCO$) might be formed simply because, upon C−Cl fission, the Cl fragment cannot escape from the original site due to the matrix cage effect so that the secondary reaction of Cl + C_2H_3CO yielded $CH_2ClCHCO$.[6] The observation of the 1,3-Cl shift channel in these two experiments was obscured by the cage effect of either the solvent or the matrix host.

Prasanta and Lee irradiated a *p*-H_2 matrix containing $CH_2CHC(O)Cl$ at 3.2 K with light at 193 nm and observed infrared (IR) absorption lines that were assigned to the 3-propenonyl ($\cdot CH_2CHCO$) radical; no line of $CH_2ClCHCO$ was observed.[13] These results are consistent with a major radical formation channel CH_2CHCO + Cl followed by escape of the Cl atom from the original site in *p*-H_2, which has a diminished cage effect. The observation of 3-propenonyl ($\cdot CH_2CHCO$) radical but not 3-propenalyl (*s-cis*- or *s-trans*-$CH_2C\dot{H}CO$) radical indicates that the former is the most stable isomer and that the barrier heights for conversion from *s-cis*- or *s-trans*-$CH_2C\dot{H}CO$ to $\cdot CH_2CHCO$ are small.

Cui et al. undertook various quantum-chemical calculations to map the potential-energy surfaces of isomerization and dissociation of $CH_2CHC(O)Cl$ in its S_0, T_1, T_2, and S_1 states.[14] They indicated that, upon excitation at 310 nm, $S_1 \rightarrow T_1$ intersystem crossing is the dominant primary process, which is followed by 1,3-Cl migration along the T_1 path, whereas, for excitation at a wavelength smaller than 230 nm, cleavage of the C−Cl bond is the exclusive primary channel, consistent with experiments.

We have reinvestigated the photodissociation of gaseous $CH_2CHC(O)Cl$ with a step-scan FTIR spectrometer and obtained emission spectra of HCl and CO much improved from the previous report.[10] We were able to identify two pathways that form HCl: the major one due to four-center HCl elimination directly from $CH_2CHC(O)Cl$, and the other from $CH_2ClCHCO$, which was produced from a 1,3-Cl shift of $CH_2CHC(O)Cl$. The latter HCl elimination occurs via a roaming pathway, so we propose a modified Franck−Condon analysis to predict the HCl vibrational energy measured in the experiments.

2. EXPERIMENTS AND COMPUTATIONS

The apparatus employed to obtain time-resolved IR emission spectra using a step-scan FTIR spectrometer coupled with a set of Welsh mirrors to collect light has been described.[15−17] The sizes of the photolysis beams at the detection center were ~11.0 × 5.5 mm^2 with a fluence ~12 mJ cm^{-2} from an ArF laser (Coherent, COMPexPro-50) at 193 nm. The transient signal detected with an InSb detector (rise time 0.22 μs) was preamplified, followed by further amplification 20−50 times (bandwidth 1 MHz) before being digitized and recorded with an external data-acquisition board (12-bit) at resolution of 25 ns. Survey spectra were recorded in the spectral range 1800−7800 cm^{-1}. Data were typically averaged over 60 laser pulses at each scan step; 1332 scan steps were performed to yield an interferogram resulting in a spectrum at resolution 12 cm^{-1}. To detect emission of CO at high resolution, we used a filter (OCLI, W05200-6X) passing 1670−2325 cm^{-1} for undersampling. Data were typically averaged over 60 laser pulses at each scan step; 2984 scan steps were performed to yield an interferogram resulting in a spectrum of resolution 0.4 cm^{-1} in the spectral region 1800−2325 cm^{-1}; the lower bound was limited by the detectivity of the InSb detector. To detect emission of HCl in the spectral region 2350−3250 cm^{-1}, we used undersampling with two IR filters (SPECTROGON, SP-4300 nm and OCLI, W03999-4) passing 2350−4830 cm^{-1} and 2005−3250 cm^{-1}, respectively. Data were typically averaged over 30 laser pulses at each scan step; 5754 scan steps were performed to yield an interferogram resulting in a spectrum of resolution 0.4 cm^{-1}. To improve the ratio of signal-to-noise (S/N) of the spectra of CO and HCl, four spectra recorded under similar experimental conditions were averaged. Typically, 40 consecutive time-resolved spectra were summed to yield spectra representing emission at intervals of 1.0 μs.

As acryloyl chloride (96%, Aldrich, containing ~400 ppm phenothiazine stabilizer) undergoes slow polymerization near 300 K, we applied a freeze−pump−thaw method to remove the impurities before preparation of a sample mixture. Acryloyl chloride was injected into the vacuum chamber as a diffusive beam through a slit-shaped inlet. The sample has a vapor pressure ~105 Torr at 298 K, and we maintained the sample at 283 K to decrease its vapor pressure to ~46 Torr. The partial pressure of $CH_2CHC(O)Cl$ in the chamber was maintained under 60 mTorr. Ar (AGA Specialty Gases, 99.999%) in a minimal pressure (~15 mTorr) was added near the entrance of the photolysis port to suppress the formation of a solid deposit on the quartz window.

Energies of stationary geometries were calculated at the G4//B3LYP/6-311++G(3df,2pd) level of theory, including zero-point correction, using the Gaussian 09 software package.[18] Intrinsic reaction coordinate simulations were performed at the B3LYP/6-311++G(3df,2pd) level of theory, with a reaction coordinate step size of 0.0279 $amu^{1/2}$ bohr, but without zero-

DOI: 10.1021/jp512376a
J. Phys. Chem. A XXXX, XXX, XXX−XXX

point correction. Molecular geometries were rendered using the Molden program.[19]

3. RESULTS

In these experiments, to maintain a nearly collisionless condition within 1-μs period, the partial pressures of $CH_2CHC(O)Cl$ and Ar were decreased as much as practicable while maintaining a satisfactory ratio of signal-to-noise. The calculated absorption cross section of $CH_2CHC(O)Cl$ at 193 nm is 4×10^{-17} cm^2 molecule^{-1}.[13] The power dependence of the emission signals was tested; the order of power dependence was determined to be 0.95 $\pm$ 0.05 for light at 193 nm with fluence <15 mJ cm^{-2}. Typically ~10% of $CH_2CHC(O)Cl$ absorbed the laser light.

Traces (a)−(c) of Figure 1 shows representative survey emission spectra in the spectral region 1800−6500 cm^{-1}

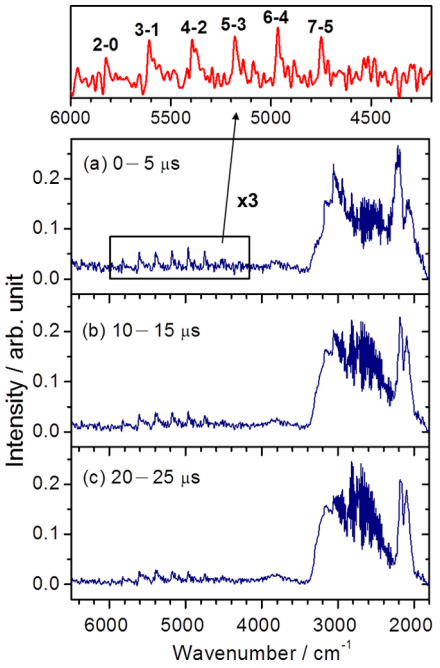

Figure 1. Emission spectra in the spectral region 1800−6500 cm^{-1} recorded 0−5 μs (a), 10−15 μs (b), and 20−25 μs (c) upon photolysis of a flowing mixture of $CH_2CHC(O)Cl$ (56 mTorr) and Ar (15 mTorr) at 193 nm. Spectral resolution is 12 cm^{-1}; 60 laser pulses were averaged at each scan step.

recorded at 5-μs intervals upon photolysis of a mixture of $CH_2CHC(O)Cl$ (56 mTorr) and Ar (15 mTorr) at 193 nm; the spectral resolution is 12 cm^{-1}. The emission in the region 2000−2300 cm^{-1} is assigned to the *P*-and *R*-branches of CO and those in regions 2300−3000 cm^{-1} and 4500−6000 cm^{-1} are assigned to the fundamental and overtone bands of HCl, respectively; emission up to v = 7 was identified from the overtone bands. A broad continuous feature in the region 2000−3400 cm^{-1} underlying the emission of CO and HCl is likely due to the C−H stretching modes of some dissociation products such as C_2H_2, C_2H_3, or C_2H_4. The unresolved structure of this feature precluded definitive assignments.

3.1. Emission of HCl. Emission spectra of HCl recorded at resolution 0.4 cm^{-1} and at 1-μs intervals for the first three μs after photolysis of $CH_2CHC(O)Cl$ (56 mTorr) in Ar (15 mTorr) are presented in Figure 2; superb ratios of signal-to-noise and slow quenching are demonstrated. Because of the

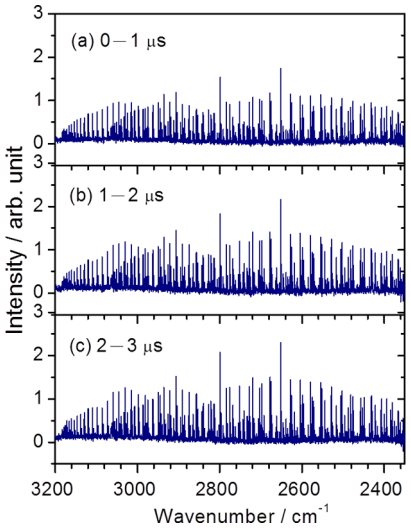

Figure 2. Emission spectra of HCl in the spectral region 2350−3200 cm^{-1} recorded 0−1 μs (a), 1−2 μs (b), and 2−3 μs (c) upon photolysis of a flowing mixture of $CH_2CHC(O)Cl$ (56 mTorr) and Ar (15 mTorr) at 193 nm. Spectral resolution is 0.4 cm^{-1}. Thirty laser pulses were averaged at each scan step; four spectra recorded under similar conditions were averaged.

narrow widths of these lines, we could easily remove the overlapping broad feature by baseline correction. The vibration−rotational assignments of each line based on spectral parameters reported by Arunan et al.[20] and Coxon and Roychowdhury[21] are shown as stick diagrams in Figure S1 of the Supporting Information. Emission of HCl up to levels $J \leq 35$ and $v \leq 7$ was observed. Each vibration−rotational line in the *P* and *R* branches was normalized with the instrument-response function, and divided by its respective Einstein coefficient[20] to yield a relative population $P_v(J)$, in which v and J represent vibrational and rotational quantum numbers of the upper states. Partially overlapped lines were curve-fitted to yield their individual intensities. Semilogarithmic plots of $P_v(J)/(2J+1)$ versus E_{rot} (in cm^{-1}) for HCl (v = 1−6), derived from the spectrum recorded in the range 0−1 μs, are shown in Figure 3. Error limits for each $P_v(J)$ were typically derived on taking into account the errors in the integration which is affected by the baseline.

The rotational distribution of HCl is non-Boltzmann. These bimodal-like rotational distributions observed for $v \leq 4$ are fitted with biexponential functions to yield two rotational temperatures, as listed in Table 1 and indicated in Figure 3; unless specified, error limits listed in this paper represent one standard deviation in fitting. As the bimodal populations of level v = 4 cannot be obtained confidently from data in 0−1 μs, we estimated the rotational temperatures of these two components upon extrapolation from data at a later period and fixed these two temperatures in the bimodal fitting. We denote these two components as high-*J* and low-*J* components. Fitted Boltzmann-like rotational distributions for the high-*J* component of HCl yielded rotational temperatures of 4800−5900 K for v = 1−4. The contribution of the low-*J* component is less than 25%, with estimated rotational temperatures in the range 680−1100 K. The rotational distributions of HCl (v = 5 and 6) are Boltzmann-like; we attribute them to the high-*J* component even though some contribution from the low-*J* component cannot be excluded.

DOI: 10.1021/jp512376a
J. Phys. Chem. A XXXX, XXX, XXX−XXX

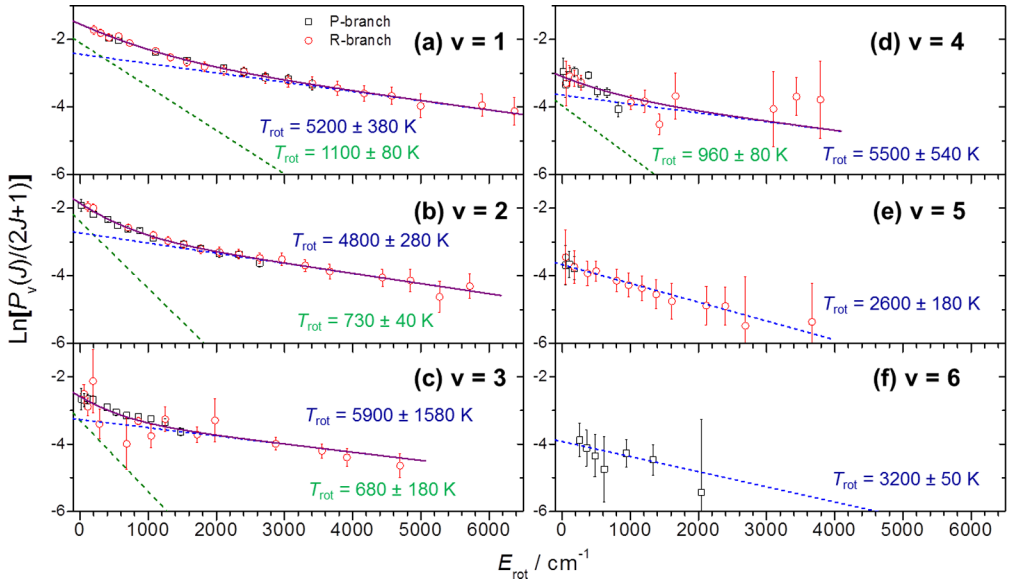

Figure 3. Semilogarithmic plots of relative rotational populations of HCl (v = 1−6) 0−1 μs after photolysis of a flowing mixture of $CH_2CHC(O)Cl$ and Ar at 193 nm (symbols ○ for the *R*-branch and □ for the *P*-branch). Solid lines represent least-squares bimodal fits. Thin dashed lines represent the low-*J* and high-*J* components.

Table 1. Summary of Observed Rotational and Vibrational Temperatures, Average Energies, and Vibrational Populations P_v of HCl in two components

	high-*J* component					low-*J* component				
	T_{rot}/K	E_{rot}/kJ mol^{-1}	T_{vib}/K	P_v/%	E_{vib}/kJ mol^{-1}	T_{rot}/K	E_{rot}/kJ mol^{-1}	T_{vib}/K	P_v/%	E_{vib}/kJ mol^{-1}
v = 0				40.1 ± 4.8[a]	0.0				51.6 ± 13.7[a]	0.0
v = 1	5200 ± 380	37.7		21.2 ± 4.2	7.3	1100 ± 80	9.3		26.2 ± 5.2	9.0
v = 2	4800 ± 280	35.3		15.1 ± 2.5	10.2	730 ± 40	6.0		13.2 ± 2.2	8.9
v = 3	5900 ± 1580	34.3		10.1 ± 2.4	10.1	680 ± 180	5.7		5.2 ± 1.3	5.2
v = 4	5500 ± 540	30.0		6.4 ± 2.7	8.4	960 ± 80	8.0		3.9 ± 1.6	5.1
v = 5	2600 ± 180	18.3		3.4 ± 1.3	5.5					
v = 6	3200 ± 50	11.0		2.5 ± 1.0	4.2					
v = 7				1.6 ± 0.4[a]	3.4					
average[b]		34 ± 5	8100 ± 470		49 ± 9		8 ± 2	4900 ± 530		28 ± 7
nascent[c]		36 ± 6			49 ± 9		9 ± 3			28 ± 7
branching[d]			0.80 ± 0.15					0.20 ± 0.05		
Yang et al.[e]	1500 ± 150	12.6	30200 ± 11710		87.0					

[a]Extrapolated values. [b]Measured from 0−1 μs. [c]Extrapolated to t = 0. [d]Branching ratio of high-*J* and low-*J* rotational components. [e]Comparison with ref 10.

We assume a Boltzmann distribution for both high-*J* and low-*J* components and associate an interpolated population with missing data due to severely overlapped lines. The average rotational energy, $E_{rot}(v)$, for each vibrational level of HCl for both low-*J* and high-*J* components determined in the period 0−1 μs, obtained on summing a product of rotational level energy and normalized population for each rotational level, are listed in Table 1. Average rotational energies of E_{rot} = 8 ± 2 kJ mol^{-1} for the low-*J* component of HCl (v = 1−4) and E_{rot} = 34 ± 5 kJ mol^{-1} for the high-*J* component of HCl (v = 1−6) are derived; the rotational energy of the v = 0 level was unable to be determined.

Although we employed the smallest practicable pressure, the rotational quenching must be considered. Similar procedures were undertaken for spectra averaged over 1−2, 2−3, and 3−4 μs; semilogarithmic plots of $P_v(J)/(2J+1)$ versus E_{rot} (in cm^{-1}) for HCl (v = 1 −6) for each period are shown in Figure S2 of the Supporting Information. The variations in rotational temperature for the high-*J* and low-*J* components of each vibrational level are depicted in Figure 4. With a short extrapolation from these data according to an exponential decay of temperature to 298 K, we estimate the nascent rotational temperature to be 1200 ± 50, 800 ± 10, 700 ± 10, and 1100 ± 60 K for the low-*J* component of v = 1−4, respectively, and 5500 ± 170, 5300 ± 120, 5800 ± 290, 6300 ± 580, 2800 ± 110, and 3200 ± 50 K for the high-*J* component of v = 1−6, respectively. The average ratios of the nascent rotational temperature to that determined at the 0−1 μs period are 1.09 ± 0.05 and 1.06 ± 0.06 for the low-*J* and high-*J* components, respectively. After applying these correction factors for rotational quenching, we derive nascent rotational energies of 9 ± 3 and 36 ± 6 kJ mol^{-1} for the low-*J* and high-*J* components of HCl, respectively.

We normalized values of $P_v = \sum_J P_v(J)$, populations obtained on counting levels up to observed maximal *J* values in each vibrational level v, to yield a relative vibrational population.

DOI: 10.1021/jp512376a
J. Phys. Chem. A XXXX, XXX, XXX−XXX

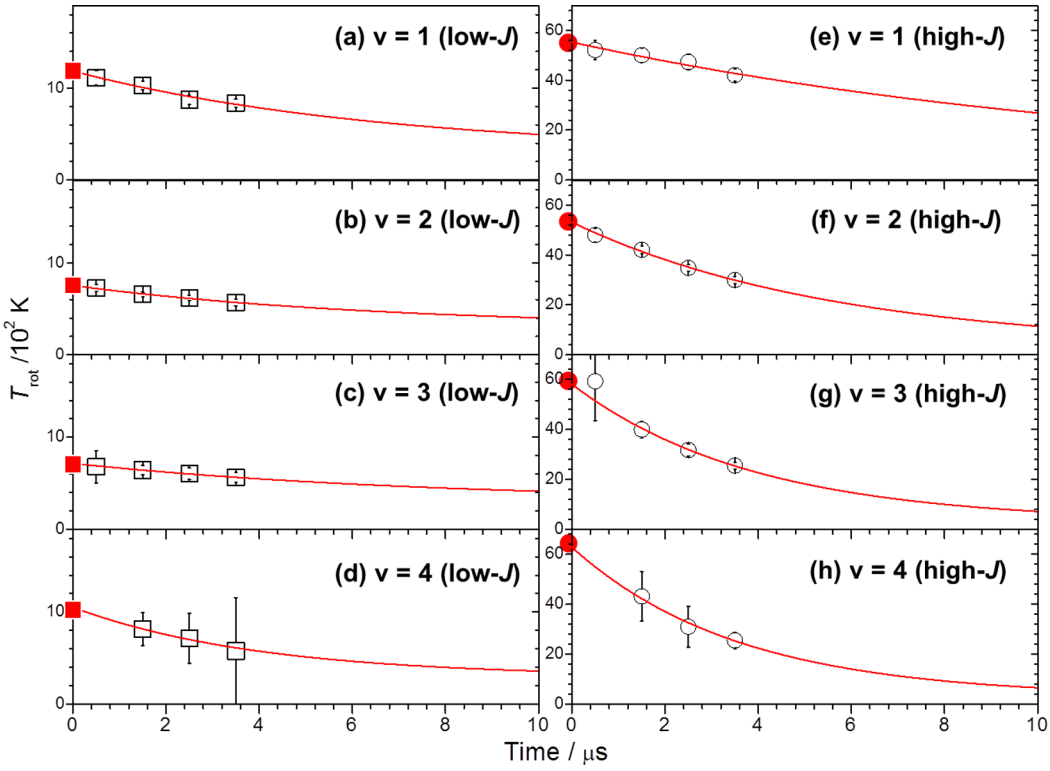

Figure 4. Plot of rotational temperature T_{rot} of the low-J and high-J components of HCl (v = 1–4) from photolysis of a flowing mixture of $CH_2CHC(O)Cl$ and Ar at 193 nm as a function of time. Solid lines represent fits with exponential decays to 298 K. The data extrapolated to t = 0 are indicated with filled symbols.

Assuming a Boltzmann vibrational distribution, we estimated the vibrational population of HCl (v = 0) to be 1.97 ± 0.52 times that of HCl (v = 1) for the low-J component. The vibrational population distribution is thus (v = 0):(v = 1):(v = 2):(v = 3):(v = 4) = (57.8 ± 13.7):(26.2 ± 5.2):(13.2 ± 2.2):(5.2 ± 1.3):(3.9 ± 1.2), as listed in Table 1 and depicted in Figure 5a; the error limits reflect the uncertainties in the vibrational–rotational populations. The vibrational temperature of the low-J component of HCl is 4900 ± 530 K, and the average vibrational energy is E_{vib} = 28 ± 7 kJ mol^{-1}. For the high-J component of HCl, we estimated the vibrational population of HCl (v = 0) and HCl (v = 7) to be 1.89 ± 0.23 and 0.08 ± 0.02 times that of HCl (v = 1), respectively. Because we observed emission in the Δv = −2 overtone sequence of HCl (v = 7), we should include its population. The distribution of vibrational population is thus (v = 0):(v = 1):(v = 2):(v = 3):(v = 4):(v = 5):(v = 6):(v = 7) = (40.1 ± 4.8):(21.2 ± 4.2):(15.1 ± 2.5):(10.1 ± 2.4):(6.4 ± 2.7):(3.4 ± 1.3):(2.5 ± 1.0):(1.6 ± 0.4), as listed in Table 1 and depicted in Figure 5b. The vibrational temperature of the high-J component of HCl is 8100 ± 470 K, and the average vibrational energy is E_{vib} = 49 ± 9 kJ mol^{-1}. Vibrational quenching of HCl during the period 0–1 μs is negligible.

3.2. Emission of CO. Representative emission spectra of CO recorded at resolution of 0.4 cm^{-1} and at 1-μs intervals after photolysis of $CH_2CHC(O)Cl$ in Ar are presented in Figure 6, with excellent ratios of signal-to-noise. The vibration–rotational assignments of each line based on spectral parameters reported by Ogilvie et al.[22] are shown as stick diagrams in Figure S3 of the Supporting Information; overlapping lines of HCl are also indicated.

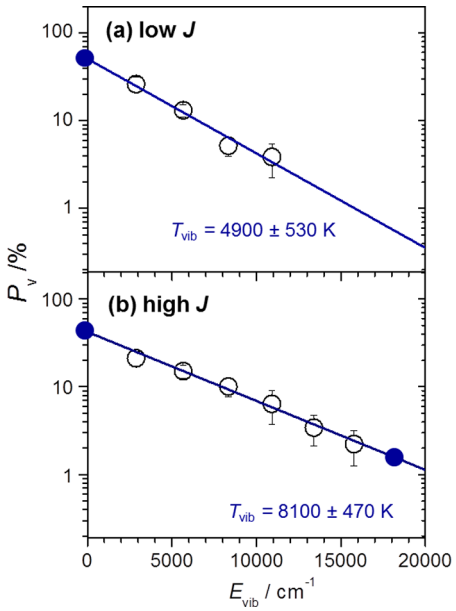

Figure 5. Relative vibrational populations of HCl produced from photolysis of a flowing mixture of $CH_2CHC(O)Cl$ and Ar at 193 nm as a function of vibrational energy: (a) low-J component and (b) high-J component. Populations indicated with the filled symbols are derived on extrapolation according to fitted Boltzmann distributions shown as solid lines.

Emission of CO from levels $J \leq 67$ and $v \leq 4$ was observed. Figure 7 presents semilogarithmic plots of $P_v(J)/(2J+1)$ versus E_{rot} (in cm^{-1}) for CO (v = 1–4), derived from the spectrum recorded in range 0–1 μs; the rotational distribution of CO is

DOI: 10.1021/jp512376a
J. Phys. Chem. A XXXX, XXX, XXX–XXX

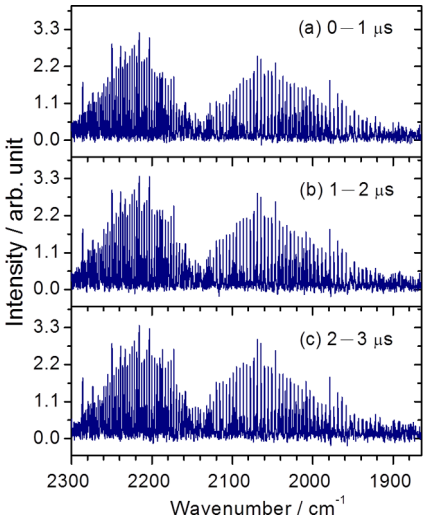

Figure 6. Emission spectra of CO in the spectral region 1865−2300 cm^{-1} recorded 0−1 μs (a), 1−2 μs (b), and 2−3 μs (c) upon photolysis of a flowing mixture of $CH_2CHC(O)Cl$ (56 mTorr) and Ar (15 mTorr) at 193 nm. Spectral resolution is 0.4 cm^{-1}. Sixty laser pulses were averaged at each scan step; four spectra recorded under similar conditions were averaged.

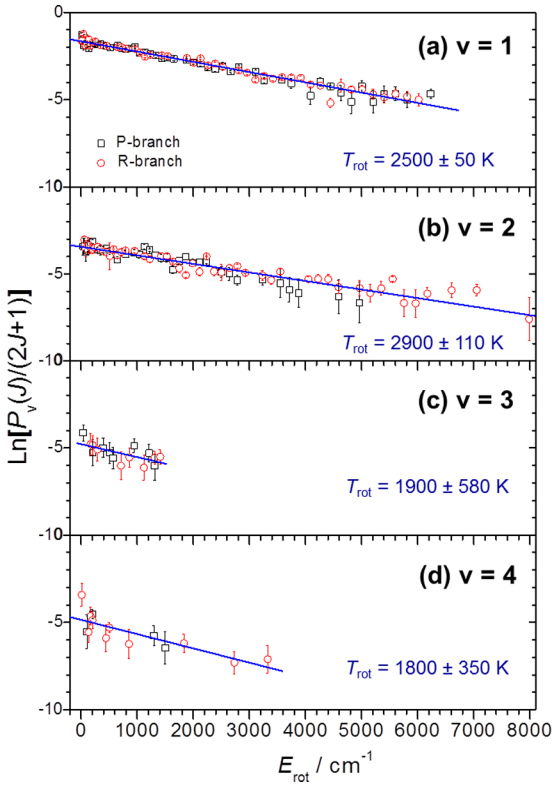

Figure 7. Semilogarithmic plots of relative rotational populations of CO (v = 1−4) 0−1 μs after photolysis of a flowing mixture of $CH_2CHC(O)Cl$ and Ar at 193 nm (symbols ○ for the *R*-branch and □ for the *P*-branch). Solid lines represent least-squares fits.

Boltzmann-like, and the rotational temperatures are indicated in Table 2. Rotational temperatures in the range 1800−2900 K were derived; the rotational distributions and temperature of CO (v = 3 and 4) are much smaller than those of CO (v = 1 and 2).

Following a similar data-processing method, we derived $E_{rot}(v)$ for each vibrational level of CO determined in period 0−1 μs and the average rotational energy E_{rot} = 20 ± 3 kJ mol^{-1} for CO (v = 1−4), as listed in Table 2; the rotational energy of the v = 0 level is unaccounted. We undertook similar procedures to correct for the rotational quenching. The spectra averaged over 1−2, 2−3, and 3−4 μs and semilogarithmic plots of $P_v(J)/(2J+1)$ versus E_{rot} (in cm^{-1}) for CO (v = 1 −4) for each period are shown in Figure S4 of the Supporting Information. The variations in rotational temperature of each vibrational level are depicted in Figure S5. The average ratio of the nascent rotational temperature of the later intervals to that determined at 0−1 μs is 1.1 ± 0.2. After applying this correction factor for rotational quenching, we derive nascent rotational energies of 21 ± 4 kJ mol^{-1} for CO.

Assuming a Boltzmann vibrational distribution, we estimated the vibrational population of CO (v = 0) to be 2.72 ± 1.38 times that of CO (v = 1). The vibrational population distribution is thus (v = 0):(v = 1):(v = 2):(v = 3):(v = 4) = (68.3 ± 34.7):(25.1 ± 3.1):(5.0 ± 1.3):(0.9 ± 0.5):(0.7 ± 0.5), as depicted in Figure 8a; the vibrational temperature is 2400 ± 500 K and the average vibrational energy of CO is E_{vib} = 10 ± 4 kJ mol^{-1}. The abrupt decrease in population of v = 3 beyond the expected uncertainty range might indicate a bimodal vibrational distribution, although the evidence is not definitive. When we employed a bimodal vibrational distribution to fit the experimental data, we derived low-v and high-v distributions with vibrational temperatures 1700 ± 600 and 20600 ± 17000 K, respectively, as depicted in Figure 8b; the population ratio of these two components is approximately (0.98 ± 0.34):(0.02 ± 0.01). This additional high-v component is consistent with a minor secondary channel, to be discussed in Section 4.2.

For the high-v component of CO, the vibrational population distribution is thus (v = 0):(v = 1):(v = 2):(v = 3):(v = 4) = (26.3 ± 12.2):(22.6 ± 2.8):(19.5 ± 5.0):(16.9 ± 9.6):(14.6 ± 9.8) as listed in Table 2. The average vibrational energy for the high-v component of CO thus derived is E_{vib} = 43 ± 18 kJ mol^{-1}. For the low-v component of CO, the vibrational population distribution is (v = 0):(v = 1):(v = 2):(v = 3) = (83.9 ± 11.0):(13.5 ± 1.7):(2.2 ± 0.6):(0.4 ± 0.2) as listed in Table 2; the average vibrational energy is E_{vib} = 5 ± 2 kJ mol^{-1}.

3.3. Theoretical Calculations. Two conformers, *s-trans*-$CH_2CHC(O)Cl$ and *s-cis*-$CH_2CHC(O)Cl$, of acryloyl chloride exist, with the former more stable by ∼1 kJ mol^{-1} than the latter.[23] Our calculations at the G4//B3LYP level show two pathways to eliminate HCl on the S_0 surface of acryloyl chloride. Both yield HCl + $H_2C{=}C{=}C{=}O$, but with very different energetics and dynamics en route. The stationary points for these pathways are shown in Figure 9. The major path involves a four-center elimination through the *s-cis* conformer with a barrier ∼209 kJ mol^{-1}. The minor path involves a sigmatropic 1,3-Cl shift from the *s-trans* conformer to 3-chloro-1-propen-1-one, $CH_2ClCHCO$, with a barrier of ∼190 kJ mol^{-1}, followed by four-center elimination over a barrier with energy ∼238 kJ mol^{-1}. This Cl-shifted product $CH_2ClCHCO$ has been reported with acryloyl chloride in a matrix[6] and in solution,[9] but the definitive evidence of the occurrence of a 1,3-Cl shift is obscured by the cage effect in matrix and in solution; whether the Cl shift occurs in the gaseous phase is not established. Yang et al. inferred[10] that this rearrangement is unlikely in the gaseous phase, based on their solution-phase experiments[9] showing that it proceeds exclusively through the T_1 state following $S_1 \rightarrow T_1$ intersystem

DOI: 10.1021/jp512376a
J. Phys. Chem. A XXXX, XXX, XXX−XXX

Table 2. Summary of Observed Rotational and Vibrational Temperatures, Average Energies, and Vibrational Populations P_v of CO

	rotation		vibration			high-v component			low-v component		
	T_{rot}/K	E_{rot}/kJ mol^{-1}	T_{vib}/K	P_v/%	E_{vib}/kJ mol^{-1}	T_{vib}/10^3 K	P_v/%	E_{vib}/kJ mol^{-1}	T_{vib}/ 10^3 K	P_v/%	E_{vib}/kJ mol^{-1}
v = 0				68.3 ± 34.7[a]	0.0		26.3	0.0		83.9	0.0
v = 1	2500 ± 50	20.0		25.1 ± 3.1	6.4		22.6	5.8		13.5	3.5
v = 2	2900 ± 110	23.0		5.0 ± 1.3	2.6		19.5	10.0		2.2	1.1
v = 3	1900 ± 580	15.6		0.9 ± 0.5	0.7		16.9	12.8		0.4	0.3
v = 4	1800 ± 350	13.2		0.7 ± 0.5	0.7		14.6	14.7			
average[b]	2300 ± 830	20 ± 3	2400 ± 500		10 ± 4						
nascent[c]	2500 ± 640	21 ± 4			10 ± 4	21 ± 17		43 ± 18	1.7 ± 0.6		5 ± 2
branching[d]							0.02 ± 0.01			0.98 ± 0.34	
Yang et al.[e]	4000 ± 500	33.1	7000 ± 1530		44.8						

[a]Extrapolated values. [b]Measured from 0−1 μs. [c]Extrapolated to t = 0. [d]Branching ratio of high-v and low-v vibrational components. [e]Reference 10.

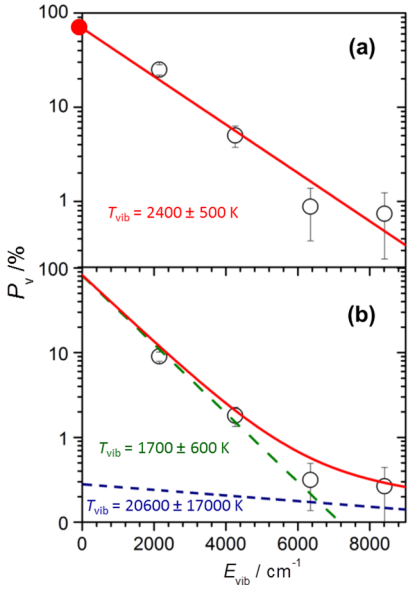

Figure 8. Relative vibrational populations of CO produced from photolysis of a flowing mixture of $CH_2CHC(O)Cl$ and Ar at 193 nm as a function of vibrational energy. (a) Fitted Boltzmann distribution shown as a solid line. Populations in v = 0 are derived by extrapolation and indicated with the filled symbol. (b) Fitted bimodal vibrational distribution shown as a solid line. The low-v and high-v components are presented as dashed lines.

crossing (ISC). They noted that Cui et al.[14] calculated the rate of this $S_1 \rightarrow T_1$ ISC to be significantly smaller than both the rate of C−Cl bond fission on the S_1 surface and the rate of $S_1 \rightarrow S_0$ internal conversion via vibronic coupling.

However, our experimental results show two pathways to eliminate HCl; the fraction (about 20%) of HCl elimination that occurs via the minor pathway is too large to be assigned to elimination following intersystem crossing (with slow $S_1 \rightarrow T_1$ ISC rate estimated in ref 14). Notably, ref 14 does not report rates for excitation wavelengths shorter than 230 nm; however, the data therein suggest increasing competitiveness of $S_1 \rightarrow S_0$ internal conversion at higher energies. Moreover, Szpunar et al. detected significant (~25%) branching to HCl from excitation at 193 nm,[7] which is not consistent with a slow $S_1 \rightarrow T_1$ ISC. We thus computationally searched for a pathway requiring internal conversion. The following computational results identify two pathways for HCl elimination on the S_0 surface.

The competition between the two HCl-elimination pathways on the potential-energy surface, involving the three local minima, transition states for both HCl elimination pathways, and transition states for the isomerization and conformation changes, were modeled as a set of five first-order rate equations: one equation for the number density as a function of time for each of the three minima and two product pathways. These equations involve six nonzero rate coefficients, namely, the forward and reverse coefficients for both the *cis*−*trans* isomerization and the Cl shift as well as the forward coefficients for the two HCl elimination pathways. These coefficients were determined with RRKM theory.[24] To calculate the sums and densities of states, we used the semiclassical technique of Whitten Rabinovitch implemented in that software.

We specifically include the possibility of the Cl atom shift over the 190 kJ mol^{-1} barrier shown in Figure 9. When we included the possibility of direct CO loss after internal conversion to S_0 in the calculation, both from acryloyl chloride and from 3-chloro-1-propen-1-one, we found the barriers were too large to affect the result significantly. The theoretical branching ratio between the two elimination channels was determined as the ratio of the populations in the product asymptote of the two HCl elimination channels in the infinite-time limit. This calculation predicts a statistical branching ratio of 0.81:0.19 for direct HCl elimination from the *s-cis* conformer: HCl elimination from 3-chloro-1-propen-1-one after the Cl shift.

Using a modified Franck−Condon approximation, we also predicted the vibrational energy that each elimination pathway would confer to the HCl product. The energies along the intrinsic reaction coordinate for the two pathways calculated at the B3LYP level of theory are plotted in Figure 10. In the figure, open red diamonds represent elimination from the *s-cis* conformer, filled blue circles represent elimination from the 1,3-Cl shifted intermediate, and energies are given relative to the B3LYP energy of the *s-cis* conformer. The energy along each reaction coordinate has a relatively flat plateau in the vicinity of the transition state, after which the Cl atom approaches the H atom to eliminate HCl. Choosing the correct geometry to predict Franck−Condon factors for the vibrational states of HCl hence required close consideration. Near the mass-weighted displacement along the reaction coordinate of $S \approx 0.5$ on the *s-cis* IRC and $S \approx 2.5$ on the Cl-shifted IRC, indicated by arrows in Figure 10, the plateau ends and the energy drops precipitously. We associate this sharp change in energy with the formation of the nascent H−Cl bond and use

DOI: 10.1021/jp512376a
J. Phys. Chem. A XXXX, XXX, XXX−XXX

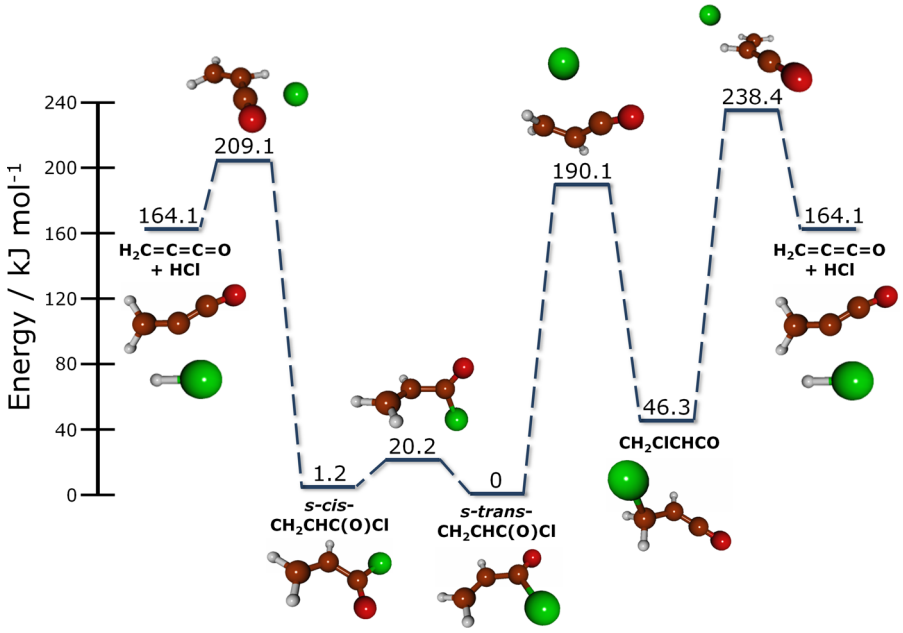

Figure 9. Minima and transition states for the two HCl-elimination channels on the S_0 surface of acryloyl chloride. Energies relative to the energy of the *s-trans* conformer are calculated at the G4//B3LYP/6-311++G(3df,2pd) level. All energies are corrected for vibrational zero-point effects.

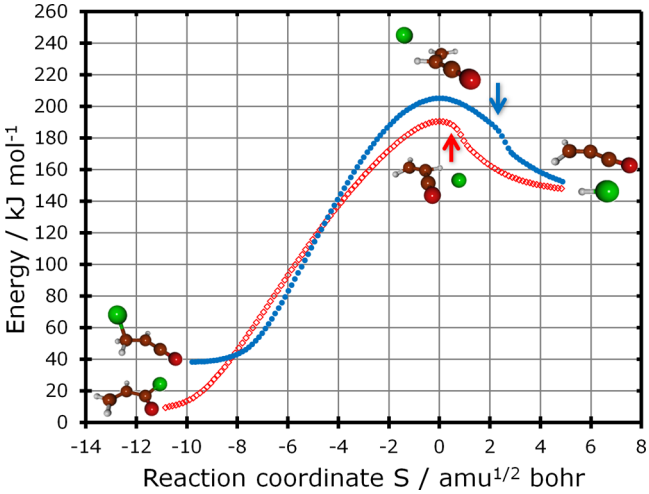

Figure 10. Intrinsic reaction coordinate (IRC) calculation for HCl elimination from the 1,3-Cl-shifted (filled blue circles) and *s-cis* (empty red diamonds) isomers. The minimum potential energy of the *s-cis* conformer without zero-point correction is chosen as zero. As IRC points were calculated at the B3LYP/6-311++G(3df,2pd) level, the barrier heights are not identical to the G4 results in Figure 9, even after zero-point correction. The geometry at the kink near S = 0.5 for *s-cis* IRC and S = 2.5 for the 1,3-Cl-shifted IRC, indicated respectively by red and blue arrows, was used for the Franck−Condon estimate of the amount of vibrational energy in the eliminated HCl molecule, as described in the text.

the H−Cl distance at that point along the reaction coordinate to approximate the vibrational energy imparted to the eliminated HCl. The coordinate at which the plateau ends corresponds to a minimum in the second derivative of energy (see Figure S6 of the Supporting Information). For the major *s-cis* elimination channel, the second derivative is minimized at S = 0.47, with an elimination H−Cl bond length of ∼1.69 Å. The Franck−Condon estimate for the HCl vibrational energy using the outer turning point of 1.69 Å gives $v \approx 7$ vibrational quanta. For the minor Cl shift channel, the plateau ends at S = 2.29, and we find a bond length of ∼1.64 Å, equivalent to $v \approx 5$ quanta in the stretch of the HCl product from that pathway.

To verify that the approximation developed in the preceding paragraph is valid, we reproduced its results using a metric other than potential energy along the reaction coordinate. Figure 11 shows the interatomic distance between the Cl and central C atom for each pathway plotted as a function of progress along the reaction coordinate. In both cases, the C−Cl separation decreases as the Cl atom approaches to abstract a hydrogen atom. We chose for our Franck−Condon approximation the distance of closest approach in Figure 11, thus assuming that the H−Cl bond is formed there, followed by the nascent HCl molecule transiting away from the propadienone cofragment. For the *s-cis* elimination channel, the C−Cl distance is minimized at coordinate S = 0.47, with an elimination H−Cl bond length of ∼1.69 Å, equivalent to $v \approx 7$. For the Cl-shifted channel, the C−Cl distance is minimized at coordinate S = 2.37, corresponding to an H−Cl bond length of ∼1.61 Å and $v \approx 5$. These results are consistent with choosing the position along the reaction coordinate for the Franck−Condon analysis for H−Cl vibration based on the drop in potential energy along the IRC. This agreement provides confidence in using these geometries for the Franck−Condon prediction for vibrational energy imparted to the HCl product. This method appears to be much more reliable than using the geometry at the formal transition state for HCl elimination from the Cl-shifted intermediate. The H−Cl bond distance at the formal transition state for that pathway is anomalously large as it is a roaming-like transition state; rather, the Cl atom must approach the CH moiety in the radical again to actually eliminate HCl.

4. DISCUSSION

In our previous experiments involving deposition of $CH_2CHC(O)Cl$ into a *p*-H_2 matrix, a ratio of 0.52 ± 0.14 for *s-cis*-$CH_2CHC(O)Cl$ to *s-trans*-$CH_2CHC(O)Cl$ was observed, corresponding to an energy difference of 1.6 ± 0.7 kJ mol^{-1}

DOI: 10.1021/jp512376a
J. Phys. Chem. A XXXX, XXX, XXX−XXX

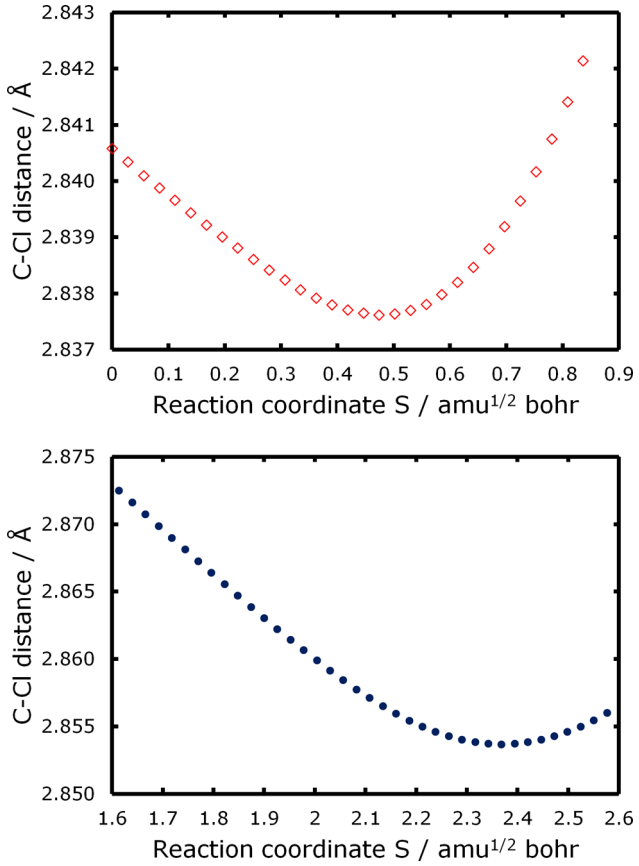

Figure 11. Distance between the C and Cl atoms involved in HCl elimination from the *s-cis* conformer (open red diamonds) and the 1,3-Cl-shifted isomer (filled blue circles). The horizontal axis is restricted to coordinates near the H abstraction event, as described in the text. The distance of closest approach of the Cl to the C atom identifies the geometry along the IRC to use for the Franck–Condon estimate for the HCl vibrational distribution.

if a Boltzmann distribution at 298 K be assumed,[13] consistent with our calculations. At large energy these two conformers are likely indistinguishable and can be considered as one species.

Upon excitation of $CH_2CHC(O)Cl$ at 193 nm (corresponding to energy 618 kJ mol^{-1}), five reaction channels are energetically possible:

$$CH_2CHC(O)Cl \rightarrow CH_2CHCO + Cl, \quad \Delta H^\circ = 342 \text{ kJ mol}^{-1} \tag{1}$$

$$CH_2CHC(O)Cl \rightarrow H_2C{=}C{=}C{=}O + HCl, \quad \Delta H^\circ = 160 \text{ kJ mol}^{-1} \tag{2}$$

$$CH_2CHC(O)Cl \rightarrow CH_2{=}CH + ClCO, \quad \Delta H^\circ = 418 \text{ kJ mol}^{-1} \tag{3}$$

$$CH_2CHC(O)Cl \rightarrow CH_2CHCl + CO, \quad \Delta H^\circ = 54.8 \text{ kJ mol}^{-1} \tag{4}$$

$$CH_2CHC(O)Cl \rightarrow CH_2ClCHCO, \quad \Delta H^\circ = 43.1 \text{ kJ mol}^{-1} \tag{5}$$

in which the listed ΔH° at 0 K are taken from ref 7. Although Cl can be produced in its ground ($^3P_{3/2}$) electronic state or its excited ($^3P_{1/2}$) state, the energy difference (10.5 kJ mol^{-1}) is too small to be resolved in either the photofragmentation translational-energy experiments or this experiment; we do not distinguish these two channels involving separate spin–orbit states of Cl. According to the results of Szpunar et al.,[7] the major channel involves C–Cl fission, reaction 1. These authors observed products Cl + C_2H_3CO in two sets with large and small kinetic energies, corresponding to dissociation on the excited and ground electronic surfaces, respectively. The C_2H_3CO radical was not detected because it had sufficient internal energy to undergo secondary decomposition to form C_2H_3 + CO. A minor channel to form $H_2C{=}C{=}C{=}O$ and HCl via a four-center elimination (reaction 2) was also observed; the branching ratio of this channel was estimated to be ~25%. Similarly, all $H_2C{=}C{=}C{=}O$ coproduct was found to have internal energy sufficient to dissociate into vinylidene (CH_2C:) and CO; vinylidene is expected to isomerize readily to C_2H_2. No evidence of the occurrence of reactions 3–5 was observed.

Because reaction 1 is the major channel, the production of HCl from secondary reactions should be considered. The rate coefficients of reactions

$$Cl + CH_2CHC(O)Cl \rightarrow HCl + C_2H_2C(O)Cl \tag{6}$$

$$Cl + CH_2CHCO \rightarrow HCl + H_2C{=}C{=}C{=}O \tag{7}$$

are unreported, but the rate coefficient of a similar reaction

$$Cl + CH_2CHC(O)OH \rightarrow \text{products} \tag{8}$$

with $k_8 = 4 \times 10^{-11}$ cm^3 molecule^{-1} s^{-1} can serve as an estimate.[25] Considering that $[CH_2CHC(O)Cl]_0 = 1.8 \times 10^{15}$ molecules cm^{-3}, the reaction is only 7% complete within 1 μs. Similarly, for $[CH_2CHCO]_0 \approx 1.4 \times 10^{14}$ molecules cm^{-3}, reaction 7 is only ~5% complete. When we add all population of HCl(v) (including the extrapolated values for $v = 0$) shown in Table S1 of the Supporting Information, we observed <7% increase in population for $t > 1$ μs; this increase in population is presumed to be the formation of HCl due to a secondary reaction. The secondary reaction of Cl to produce HCl is hence negligible under our experimental conditions.

4.1. Mechanism for Formation of HCl. According to the commonly presented mechanism above, only reaction 2 can yield HCl, via a four-center elimination on the ground electronic surface. Yang et al. observed highly vibrationally excited HCl with E_{vib} = 87.0 kJ mol^{-1} and much less rotational excitation with E_{rot} = 12.6 kJ mol^{-1};[10] they did not report the detailed internal state-distribution and the presence of two rotational distributions, as we observed, because they were comparing only simulated spectra with their observations, and significant deviations exist in the presented figures. We observed two channels to produce HCl: the high-J component with $v = 1$–7 has average $E_{vib} = 49 \pm 9$ kJ mol^{-1} and $E_{rot} = 36 \pm 6$ kJ mol^{-1}, and the low-J component with $v = 1$–4 has average $E_{vib} = 28 \pm 7$ kJ mol^{-1} and $E_{rot} = 9 \pm 3$ kJ mol^{-1}; the population fractions of the high-J component: low-J component is ~0.80:0.20. Because of our much improved ratio of signal-to-noise and our detailed analysis of the distribution of internal states, we contend that our results are more reliable than those reported by Yang et al.[10] Our results of HCl with internal energy ~85 ± 11 kJ mol^{-1} for the high-J component are consistent with the red shift of ~96 kJ mol^{-1} observed in the

DOI: 10.1021/jp512376a
J. Phys. Chem. A XXXX, XXX, XXX–XXX

photoionization efficiency plot for HCl produced in UV-irradiated $CH_2CHC(O)Cl$.[7]

The high-J component of HCl is typically observed in a four-center elimination channel in chloroalkenes upon UV photodissociation. In photolysis of vinyl chloride (CH_2CHCl) at 193 nm, emission of HCl ($v \leq 7$, $J \leq 32$) was observed, with a high-J component of E_{vib} = 74 ± 3 kJ mol^{-1} and E_{rot} = 47 ± 2 kJ mol^{-1} and a low-J component of E_{vib} = 81 ± 2 kJ mol^{-1} and E_{rot} = 3.8 ± 0.3 kJ mol^{-1}; the vibrational distribution is inverted at v = 2 for the low-J component.[26,27] This bimodal distribution is because both three-center and four-center HCl elimination occurs. Martínez-Núñez et al. predicted that HCl produced from four-center elimination is more rotationally excited than that from three-center elimination.[28,29] In photolysis of 2-chloropropene ($H_2CCClCH_3$) at 193 nm, two four-center HCl-elimination channels might occur:

$$H_2CCClCH_3 + h\nu \rightarrow HCl + HC{\equiv}CCH_3, \quad \Delta H^\circ = 105 \text{ kJ mol}^{-1} \tag{9}$$

$$H_2CCClCH_3 + h\nu \rightarrow HCl + H_2C{=}C{=}CH_2, \quad \Delta H^\circ = 109 \text{ kJ mol}^{-1} \tag{10}$$

Chang et al. observed both the high-J (major) and low-J (minor) components of HCl ($v \leq 6$) with average internal energies E_{vib} = 86 ± 5 kJ mol^{-1} and $E_{rot} = 39 \pm {}^{11}_{3}$ kJ mol^{-1}; the vibrational distribution is inverted at v = 2.[30] The observed rotational distributions qualitatively fit a similar distribution for both channels obtained with quasi-classical trajectories (QCT) and the observed vibrational distribution agrees satisfactorily also with the total distribution obtained according to a weighted sum of predicted contributions from both four-center elimination channels. The major high-J component of HCl observed in this work might thus be due to the four-center elimination of $CH_2CHC(O)Cl$ (reaction 2).

Our theoretical calculations predict that two paths exist to eliminate HCl on the S_0 surface of acryloyl chloride: the major path is a four-center elimination through the *s-cis* conformer, and the minor path involves a 1,3-Cl shift from the *s-trans* conformer to $CH_2ClCHCO$ (reaction 5), followed by four-center elimination:

$$CH_2ClCHCO \rightarrow H_2C{=}C{=}C{=}O + HCl, \quad \Delta H^\circ = 118 \text{ kJ mol}^{-1} \tag{11}$$

Our statistical prediction for the branching ratio between these two pathways, 0.81:0.19, agrees well with the experimental result of 0.80:0.20, indicating that the observed major channel is to be associated with elimination from the *s-cis* conformer, and the minor channel with elimination from a 1,3-Cl-shifted geometry.

The calculations explain also the bimodal vibrational distribution of quantum states measured for the HCl product. For the *s-cis* elimination channel, the H−Cl bond length of ∼1.69 Å at the minimum C−Cl distance along the elimination reaction coordinate corresponds to excitation to $v \approx 7$ of HCl, whereas for the 1,3-Cl shifted channel, the H−Cl bond length of ∼1.61 Å at the minimum C−Cl distance along the elimination reaction coordinate corresponds to excitation to $v \approx 5$ of HCl. This result agrees qualitatively with our experimental observation of up to v = 7 for our major channel and v = 4 for our minor channel, reinforcing our identification of the major channel with HCl elimination from the *s-cis* conformer and the minor channel with elimination from the 1,3-Cl-shifted intermediate. We note that this Franck−Condon analysis does not make the traditional choice of using the H−Cl distance at the formal transition state, as that distance is not meaningful for reactions characterized by roaming. Rather, we introduce a procedure for identifying the correct point along the IRC to generate the Franck−Condon prediction, the point at which the roaming Cl atom has reapproached the C atom to which the H atom is attached. At this point, the energy along the IRC also drops sharply as the H−Cl bond is formed.

One may briefly consider why both prior experimental studies[7,10] of the gas phase photodissociation of acryloyl chloride at 193 nm show that, while C−Cl fission on S_1 is the major channel, the HCl elimination channel following $S_1 \rightarrow S_0$ internal conversion also contributes significantly to the product branching. The theoretical study of Cui et al.[14] attempted to estimate the rate constants for C−Cl photofission on S_1, for intersystem crossing, and for internal conversion to S_0. They concluded that both intersystem crossing and the internal conversion processes are minor at an excitation energy of 519 kJ mol^{-1} (the calculations did not extend to 618 kJ mol^{-1}, the energy of a 193 nm photon). However, Cui et al. only considered internal conversion at the geometry of the S_1 minimum, where the energy gap between S_1 and S_0 is large. Excitation at 193 nm gives access to a wider range of geometries on the S_1 potential energy surface, so it might result in a larger internal conversion rate if a region with a smaller energy gap becomes accessible.

4.2. Mechanism for Formation of CO. According to the results of Szpunar et al.,[7] both CH_2CHCO produced from two channels of reactions 1 and $H_2C{=}C{=}C{=}O$ produced from reaction 2 or 11, respectively, have internal energy sufficient to form CO and coproducts,

$$CH_2CHCO \rightarrow CH_2{=}CH + CO, \quad \Delta H^\circ = 84.9 \text{ kJ mol}^{-1} \tag{12}$$

$$H_2C{=}C{=}C{=}O \rightarrow CH_2{=}C{:} + CO, \quad \Delta H^\circ = 168 \text{ kJ mol}^{-1} \tag{13}$$

in which the listed ΔH° values at 0 K are taken from ref 7. CO might consequently be produced from four distinct channels, each with a varied distribution of internal states, but we observed a near-Boltzmann rotational distribution of CO, indicating that CO produced from these four channels has a similar rotational distribution; we are unable to distinguish these channels according to their rotational distributions.

As discussed in Section 3.2, the product CO might have two vibrational distributions with E_{vib} = 5 ± 2 and 43 ± 18 kJ mol^{-1}; the branching ratio of low-v and high-v components is approximately 0.98:0.02. Employing the branching ratio of 3.18:1 for production of Cl:HCl estimated by Szpunar et al.[7] and the branching ratio of 0.8:0.2 for the two HCl channels, we derive the branching ratio for reactions 1:2:5 followed by reaction 11 to be 76:19:5 on assuming that HCl observed by Szpunar et al. arises from both reaction 2 and reactions 5 followed by 11. Because the internal energy of HCl produced from this channel, ∼37 kJ mol^{-1}, is much smaller than the energy of ∼85 kJ mol^{-1} for HCl produced from reaction 2, the coproduct $H_2C{=}C{=}C{=}O$ produced from this channel is expected to have a greater internal energy; the secondary

DOI: 10.1021/jp512376a
J. Phys. Chem. A XXXX, XXX, XXX−XXX

dissociation product CO in this channel is consequently expected to have greater internal energy. Considering the branching ratio of ~0.05 and the greater internal energy, the observed high-v channel of CO might be associated with secondary dissociation of $H_2C{=}C{=}C{=}O$ that was produced from reactions 5 and 11.

5. CONCLUSION

We have recorded vibration−rotationally and temporally resolved emission spectra of HCl ($v \leq 7$, $J \leq 35$) in the spectral region 2350−3250 cm^{-1} and of CO ($v \leq 4$, $J \leq 67$) in the region 1865−2300 cm^{-1} upon photodissociation of gaseous $CH_2CHC(O)Cl$ at 193 nm. With a much-improved ratio of signal-to-noise and careful analysis of the distributions of internal states of HCl and CO, we derived results significantly different from those previously reported using a similar technique.[10] The HCl emission shows a minor low-J component for $v \leq 4$ with average internal energies E_{rot} = 9 ± 3 and E_{vib} = 28 ± 7 kJ mol^{-1} and a major high-J component for $v \leq 7$ with E_{rot} = 36 ± 6 and E_{vib} = 49 ± 9 kJ mol^{-1}; the branching ratio of these two channels is ~0.20:0.80. According to quantum-chemical calculations with the G4//B3LYP/6-311++G(3df,2pd) method, the former corresponds to the four-center HCl-elimination of $CH_2ClCHCO$ (reaction 11), following a 1,3-Cl shift of $CH_2CHC(O)Cl$ (reaction 5), whereas the latter corresponds to the direct four-center HCl-elimination of $CH_2CHC(O)Cl$ (reaction 2). Four possible channels are expected for CO produced from the secondary dissociation of C_2H_3CO and $H_2C{=}C{=}C{=}O$, each produced from two possible dissociation channels of $CH_2CHC(O)Cl$, but we observed a near-Boltzmann rotational distribution of CO with average rotational energy E_{rot} = 21 ± 4 kJ mol^{-1} and vibrational energy E_{vib} = 10 ± 4 kJ mol^{-1}; the vibrational distribution might be characterized with a major low-v component and a minor high-v component. The CO produced from secondary decomposition of $H_2C{=}C{=}C{=}O$ that was produced via reactions 5 and 11 might be associated with the minor high-v component, whereas the distributions of internal states of CO produced from the other three channels are indistinguishable and associated with the major low-v component.

■ ASSOCIATED CONTENT

Supporting Information

Population variation of HCl as a function of time (Table S1); spectrum and assignment of HCl (Figure S1) and CO (Figure S3),; rotational distributions of HCl(v), v = 1−6 (Figure S2), and CO(v), v = 1−4 (Figure S4), for periods 0−1, 1−2, and 2−3 μs; rotational temperature of CO as a function of time (Figure S5); and second derivatives of internal energy with reaction coordinate for the two HCl elimination pathways (Figure S6). This material is available free of charge via the Internet at http://pubs.acs.org.

■ AUTHOR INFORMATION

Corresponding Authors

*E-mail: yplee@mail.nctu.edu; Tel: +886-3-5131459; FAX: +886-3-5713491 (Y.-P.L.).

*E-mail: L-Butler@uchicago.edu; Tel: +1-773-702-7206 (L.J.B.).

Notes

The authors declare no competing financial interest.

■ ACKNOWLEDGMENTS

Ministry of Science and Technology, Taiwan (Grant No. MOST103-2745-M-009-001-ASP) and Ministry of Education, Taiwan ("Aim for the Top University Plan" of National Chiao Tung University) supported this work. The computational work was supported by the Chemical Sciences, Geosciences, and Biosciences Division, Office of Basic Energy Sciences, Office of Science, U.S. Department of Energy, under Grant No. DE-FG02-92ER14305.

■ REFERENCES

(1) Yang, Y. S.; Qi, G. R.; Qian, J. W.; Yang, S. L. Acryloyl Chloride Polymer. *J. Appl. Polym. Sci.* **1997**, *68*, 665−670.

(2) Ferrié, L.; Bouzbouz, S.; Cossy, J. Acryloyl Chloride: An Excellent Substrate for Cross-Metathesis. A One-Pot Sequence for the Synthesis of Substituted α,β-Unsaturated Carbonyl Derivatives. *Org. Lett.* **2009**, *11*, 5446−5448.

(3) van Zanden, J. J.; de Mul, A.; Wortelboer, H. M.; Usta, M.; van Bladeren, P. J.; Rietjens, I. M. C. M.; Cnubben, N. H. P. Reversal of in vitro Cellular MRP1 and MRP2-Mediated Vincristine Resistance by the Flavonoid Myricetin. *Biochem. Pharmacol.* **2005**, *69*, 1657−1665.

(4) Billard, T. Synthetic Applications of β-Fluoroalkylated α,β-Unsaturated Carbonyl Compounds. *Chem.—Eur. J.* **2006**, *12*, 974−979.

(5) Arendt, M. F.; Browning, P. W.; Butler, L. J. Emission Spectroscopy of the Predissociative Excited State Dynamics of Acrolein, Acrylic Acid, and Acryloyl Chloride at 199 nm. *J. Chem. Phys.* **1995**, *103*, 5877−5885.

(6) Piétri, N.; Monnier, M.; Aycard, J.-P. Photolysis of Matrix-Isolated Acryloyl Chloride: 1,3 Chlorine Migration and Further Evolutions. *J. Org. Chem.* **1998**, *63*, 2462−2468.

(7) Szpunar, D. E.; Miller, J. L.; Butler, L. J.; Qi, F. 193-nm Photodissociation of Acryloyl Chloride to Probe the Unimolecular Dissociation of CH_2CHCO Radicals and CH_2CCO. *J. Chem. Phys.* **2004**, *120*, 4223−4230.

(8) Lau, K.-C.; Liu, Y.; Butler, L. J. Probing the Barrier for $CH_2CHCO \rightarrow CH_2CH + CO$ by the Velocity Map Imaging Method. *J. Chem. Phys.* **2005**, *123*, 054322.

(9) Wu, W.; Liu, K.; Yang, C.; Zhao, H.; Wang, H.; Yu, Y.; Su, H. Reaction Mechanisms of a Photo-Induced [1,3] Sigmatropic Rearrangement via a Nonadiabatic Pathway. *J. Phys. Chem. A* **2009**, *113*, 13892−13900.

(10) Yang, C.; Wu, W.; Liu, K.; Wang, H.; Su, H. Photodissociation of Acryloyl Chloride in the Gas Phase. *Sci. Chin. Chem.* **2012**, *55*, 359−367.

(11) Lee, H.; Nam, M.-J.; Choi, J.-H. Ab initio Investigations of the Radical−Radical Reaction of $O(P^3) + C_3H_3$. *J. Chem. Phys.* **2006**, *124*, 044311.

(12) Cooksy, A. L. Relocalization in Floppy Free Radicals: Ab Initio Calculations of the C_3H_3O Isomers. *J. Phys. Chem. A* **1998**, *102*, 5093−5099.

(13) Das, P.; Lee, Y.-P. Infrared Absorption of 3-Propenonyl (CH_2CHCO) Radical Generated upon Photolysis of Acryloyl Chloride [$CH_2CHC(O)Cl$] in Solid para-H_2. *J. Chem. Phys.* **2013**, *139*, 084320.

(14) Cui, G.-L.; Li, Q.-S.; Zhang, F.; Fang, W.-H.; Yu, J.-G. Combined CASSCF and MR-CI Study on Photoinduced Dissociation and Isomerization of Acryloyl Chloride. *J. Phys. Chem. A* **2006**, *110*, 11839−11846.

(15) Yeh, P.-S.; Leu, G.-H.; Lee, Y.-P.; Chen, I.-C. Photodissociation of HNO_3 at 193 nm: Near-Infrared Emission of NO Detected by Time-Resolved Fourier Transform Spectroscopy. *J. Chem. Phys.* **1995**, *103*, 4879−4886.

(16) Lin, S.-R.; Lee, Y.-P. Photodissociation of 1,1-Difluoroethene-(CH_2CF_2) at 193 nm Monitored with Step-Scan Time-Resolved Fourier-Transform Infrared Emission Spectroscopy. *J. Chem. Phys.* **1999**, *111*, 9233−9241.

DOI: 10.1021/jp512376a
J. Phys. Chem. A XXXX, XXX, XXX−XXX

(17) Bagchi, A.; Huang, Y.-H.; Xu, Z. F.; Raghunath, P.; Lee, Y. T.; Ni, C.-K.; Lin, M. C.; Lee, Y.-P. Photodissociation Dynamics of Benzaldehyde (C_6H_5CHO) at 266, 248, and 193 nm. *Chem.—Asian J.* **2011**, *6*, 2961−2976.
(18) Frisch, M. J.; Trucks, G. W.; Schlegel, H. B. et al. *GAUSSIAN 09*, revision A02; Gaussian, Inc., Wallingford, CT, 2009.
(19) Schaftenaar, G.; Noordik, J. H. Molden: A Pre- and Post-Processing Program for Molecular and Electronic Structures. *J. Comput.-Aided Mol. Design* **2000**, *14*, 123−134.
(20) Arunan, E.; Setser, D. W.; Ogilvie, J. F. Vibration-Rotational Einstein Coefficients for HF/DF and HCl/DCl. *J. Chem. Phys.* **1992**, *97*, 1734−1741.
(21) Coxon, J. A.; Roychowdhury, U. K. Rotational Analysis of the $B^1\Sigma^+ \rightarrow X^1\Sigma^+$ System of $H^{35}Cl$. *Can. J. Phys.* **1985**, *63*, 1485−1497.
(22) Ogilvie, J. F.; Cheah, S.-L.; Lee, Y.-P.; Sauer, S. P. A. Infrared Spectra of CO in Absorption and Evaluation of Radial Functions for Potential Energy and Electric Dipolar Moment. *Theor. Chem. Acc.* **2002**, *108*, 85−97.
(23) Hagen, K.; Hedberg, K. Conformational Analysis. 8. Propenoyl Chloride. An Electron-Diffraction Investigation of the Molecular Structure, Composition, Syn−Anti Energy and Entropy Differences, and Potential Hindering Internal Rotation. *J. Am. Chem. Soc.* **1984**, *106*, 6150−6155.
(24) Hase, W. L.; Bunker, D. L. *Quantum Chemistry Program Exchange*, Program No. 234; Indiana University: Bloomington, IN, 1974.
(25) Aranda, A.; Martínez, E.; de Mera, Y. D.; Rodríguez, A.; Rodríguez, D.; Cuartero, J. Low-Pressure Study of the Reactions of Cl Atoms with Acrylic Acid and Allyl Alcohol. *Atmos. Environ.* **2003**, *37*, 4361−4369.
(26) Lin, S.-R.; Lin, S.-C.; Lee, Y.-C.; Chou, Y.-C.; Chen, I.-C.; Lee, Y.-P. I. Three-Center versus Four-Center HCl-Elimination in Photolysis of Vinyl Chloride at 193 nm: Bimodal Rotational Distribution of HCl ($v \leq 7$) Detected with Time-Resolved Fourier-Transform Spectroscopy. *J. Chem. Phys.* **2001**, *114*, 160−168.
(27) Bahou, M.; Lee, Y.-P. Photodissociation Dynamics of Vinyl Chloride Investigated with a Pulsed Slit-Jet and Time-Resolved Fourier-Transform Spectroscopy. *Aus. J. Chem.* **2004**, *57*, 1161−1164.
(28) Martínez-Núñez, E.; Fernández-Ramos, A.; Vázquez, S. A.; Aoiz, F. J.; Bañares, L. A Direct Classical Trajectory Study of HCl Elimination from the 193 nm Photodissociation of Vinyl Chloride. *J. Phys. Chem. A* **2003**, *107*, 7611−7618.
(29) Martínez-Núñez, E.; Vázquez, S. A.; Aoiz, F. J.; Bañares, L.; Castillo, J. F. Further Investigation of the HCl Elimination in the Photodissociation of Vinyl Chloride at 193 nm: A Direct MP2/6-31G(d,p) Trajectory Study. *Chem. Phys. Lett.* **2004**, *386*, 225−232.
(30) Chang, C.-M.; Huang, Y.-H.; Liu, S.-Y.; Lee, Y.-P.; Pombar-Pérez, M.; Martínez-Núñez, E.; Vázquez, S. A. Internal Energy of HCl upon Photolysis of 2-Chloropropene at 193 nm Investigated with Time-Resolved Fourier-Transform Spectroscopy and Quasiclassical Trajectories. *J. Chem. Phys.* **2008**, *129*, 224301.

DOI: 10.1021/jp512376a
J. Phys. Chem. A XXXX, XXX, XXX−XXX